



# Broadband Microwave Photonic Frequency Measurement Based on Optical Spectrum Manipulation and Stimulated Brillouin Scattering

Shirui Du , Xiaotong Liu, Pengfei Du, Dangwei Wang, Bo Ma, Dongyu Li, Yibei Wang, Jin Zhang, Yalan Wang, and Anle Wang 

**Abstract**—In this article, a broadband frequency measurement system based on optical spectrum manipulation and stimulated Brillouin scattering (SBS) is proposed and experimentally demonstrated, which can implement wide-range and high-resolution frequency measurement, and generate corresponding broadband interference signals in some frequency bands, that is, it has versatility. Since the frequency range of the pump light to excite SBS is expanded based on the optical spectrum manipulation and high resolution is ensured by the narrow scattering spectrum of SBS, high-resolution spectrum measurement covering a wide frequency band is finally implemented. In addition, the double sideband pump light can be used as the source of electronic interference signal. In the experiments, the frequency measurement range of the proposed system is tested to be 0.03–44 GHz, and the resolution is up to 3 MHz. Furthermore, the frequency measurement and electronic interference sharing the same work band can be carried out in the ranges of 6.3367–7.8367 GHz and 20.36–22.16 GHz.

**Index Terms**—Microwave photonic frequency measurement, interference signal generation, optical spectrum manipulation, stimulated Brillouin scattering, wide frequency range, high resolution.

## I. INTRODUCTION

**F**REQUENCY measurement is the key point of radar electronic reconnaissance and serves for radar electronic countermeasure (ECM). The reliability of the information obtained by frequency measurement directly affects the formulation of combat strategy [1]. With the development of modern radar, the common working frequency band of radar has covered 220 MHz–35 GHz [2], which requires the frequency measurement

system has the ability of high-resolution frequency measurement on the basis of wide-range frequency measurement. At the same time, the electromagnetic environment on the modern battlefield is increasingly complex, which requires the frequency measurement system to have the ability of anti-electromagnetic interference and multi-frequency measurement. Traditional electronic frequency measurement methods have the characteristics of high resolution and flexibility, but due to the bottleneck of electronic devices, they are difficult to measure broadband signals above 18 GHz, and are vulnerable to electromagnetic interference (EMI) [3], [4], which gradually fail to meet the frequency measurement requirements in the complex electromagnetic environment. Compared with electronic technology, microwave photonic technology has incomparable advantages on its well-known features, such as high frequency, wide band, immunity to electromagnetic interference and small size [5], [6]. In recent years, this technology has been extensively researched, and the frequency measurement based on it has attracted much attention [7], [8], [9], [10].

According to the information extraction mechanism, the main microwave photonic frequency measurement (MPFM) technologies can be divided into two categories [4], which are based on frequency-to-amplitude mapping [11], [12], [13], [14], [15], [16], [17], [18], [19], [20], [21], [22] or frequency-to-time mapping [23], [24]. The main principle of the technology based on frequency-to-amplitude mapping is to stimulate power change depending on frequency through various methods, establish the mapping relationship between frequency and power, and finally achieve the measurement of frequency by measuring optical power or electric power after frequency beating. The power change depending on frequency can be caused by dispersion [11], [12] or using filter [13], [14] with specific frequency responses. The method [15] based on four wave mixing can realize a high frequency measurement range from 0.04 GHz to 40 GHz. The shortcoming of this scheme is that the accuracy can only achieve 100 MHz, and it can only realize the measurement of single frequency. The accuracy of the frequency measurement methods [9], [16], [17], [18], [19], [20], [21], [22], [23] based on SBS can reach 1 MHz, one of which can realize the maximum frequency measurement range of 9–38 GHz [19], and multi-frequency measurement. The principle of the technology based on frequency-to-time mapping is to establish the mapping

Manuscript received 28 October 2022; revised 1 February 2023; accepted 28 February 2023. Date of publication 3 March 2023; date of current version 10 March 2023. This work was supported in part by NSFC Program under Grant 62001511 and in part by the National Key Research and Development Project under Grant 2018YFB2201903. (Shirui Du and Xiaotong Liu contributed equally to this work.) (Corresponding author: Anle Wang.)

Shirui Du, Xiaotong Liu, Pengfei Du, Dangwei Wang, Bo Ma, Dongyu Li, Jin Zhang, Yalan Wang, and Anle Wang are with the Air Force Early Warning Academy, Wuhan 430019, China (e-mail: d724252780@126.com; 136040-78811@139.com; wh\_dp@163.com; wdwyjxy@126.com; mabo613@163.com; li\_dongyuu@163.com; zj\_mwp@163.com; ylwang\_opt@126.com; anle-hit@163.com).

Yibei Wang is with the Hubei Key Laboratory of Ferroelectric and Dielectric Materials and Devices, Faculty of Physics and Electronic Science, Hubei University, Wuhan 430062, China (e-mail: wyb\_981030@163.com).

Digital Object Identifier 10.1109/JPHOT.2023.3251974

relationship between the frequency and time through various methods, and finally achieve the measurement by recording the occurrence moment of the specific phenomena, which can be realized by dispersion [24] or a frequency shifting recirculating delay line loop [25]. This kind of method can realize multi-frequency measurement, but its accuracy can only reach hundreds of MHz. Though the techniques based on the photonic radio-frequency (RF) channelization can be introduced into the schemes mentioned above to improve the resolution to MHz level [8], the equalization between operating range, measurement time, channel width and system simplification are still the challenge [26]. In conclusion, the scheme based on SBS and frequency-to-time mapping have the ability of multi-frequency measurement, which meets the requirements of complex electromagnetic environment. Among them, the accuracy of the schemes based on SBS can generally reach 30 MHz or even high, which is mainly attributed to the narrow scattering spectrum of SBS. Compared with other microwave photonic frequency measurement methods, they have great advantages, and have become a research hotspot.

The principle of the frequency measurement method based on SBS [9], [10], [17], [27], [28] is that the SBS is used to generate selective gain or loss on the first-order sideband of phase-modulated signal which is related to the frequency of the signal to be measured, so as to complete the PM-to-AM conversion, build the mapping relationship between frequency and power, and finally obtain the frequency to be measured by detecting the microwave signal power after frequency beating. While the range of 0.03-40 GHz is increasingly used in the existing radar, it is more meaningful for carrying out accurate measurement in this frequency band. However, there is no frequency measurement scheme based on SBS, which can achieve frequency measurement range covering the frequency band mentioned above with MHz resolution. Moreover, the above studies do not consider realizing frequency measurement and other ECM functions in a same system architecture. While frequency measurement serves radar ECM, the research of multi-functional frequency measurement system is conducive to reduce the volume and cost of the whole radar ECM system.

In this article, a wide-range and high-resolution frequency measurement method based on optical spectrum manipulation and SBS is proposed. This method can measure the frequency of microwave signal with high resolution in the frequency range covering common radar frequency bands, and produce suppression jamming signal in some frequency bands, so as to realize electronic jamming. The main difference between this method and other frequency measurement methods based on SBS is that a flexibly tunable double-sideband pump light in a large frequency range is generated through the combination of optical domain cascade phase modulation and filtering, which can ensure a wide range of frequency measurement. At the same time, a tunable broadband interference signal in certain frequency bands can be generated after frequency beating of the double-sideband pump light, to ensure the implementation of targeted electronic attack after frequency measurement. It provides a new method to realize wide-range and high-resolution

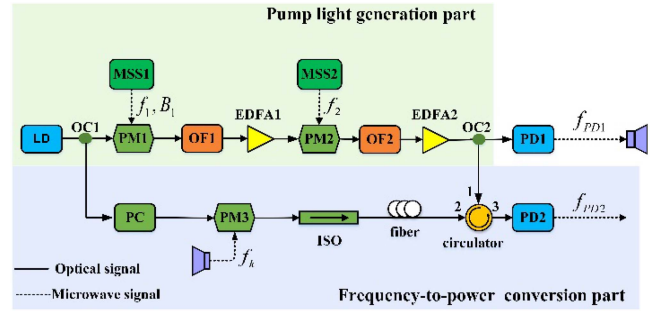


Fig. 1. Principle diagram of multifunctional frequency measurement system. LD: laser diode; PM: phase modulator; OF: optical filter; EDFA: erbium-doped fiber amplifier; MSS: microwave signal source; PD: photodetector; ISO: isolator; PC: polarization controller.

frequency measurement in complex electromagnetic environment and carry out electronic attack in some frequency bands.

## II. PRINCIPLE

As shown in Fig. 1, the proposed method is composed of a pump light generation part (shown in a light green rectangle) and a frequency-to-power conversion part (shown in a light purple rectangle). The pump light generation part uses the combination of cascade phase modulation and optical filtering to generate the required broadband tunable double-sideband optical signal. The double-sideband optical signal is used as the pump light to excite SBS during frequency measurement, or can generate the broadband interference signal with tunable frequency after frequency beating by a photodetector (PD). The frequency-to-power conversion part is realized by the selective gain and loss of SBS on the sideband of the phase-modulated signal, so as to establish the mapping relationship between frequency and power.

### A. Pump Light Generation Part Based on Optical Spectrum Operation

The double sideband pump light generation part is composed of a laser diode (LD), an optical coupler (OC1), two phase modulators (PM1, PM2), two optical filters (OF1, OF2), two erbium-doped fiber amplifiers (EDFA1, EDFA2) and two microwave signal sources (MSS1, MSS2). The spectrum evolution in the double sideband pump light generation part is shown in Fig. 2. The single-frequency continuous light generated by LD (assuming the frequency is  $f_c$ ) is used as the optical carrier of PM1. MSS1 generates microwave signal (assuming the center frequency is  $f_{1c}$  and bandwidth is  $B_1$ ) as the RF input of PM1 to generate a series of optical sidebands, as shown in Fig. 2(a). OF1, a dual-band pass filter, is employed to select the desired pair of sidebands (assuming the order is  $N$ ) from the phase-modulated signal generated by PM1, the frequencies and bandwidths of which can be expressed as  $f_c \pm Nf_1$  and  $NB_1$ , respectively, as shown in Fig. 2(b). Then, these two sidebands are modulated again by another single frequency microwave signal (assuming the frequency is  $f_2$ ) generated by MSS2 and thus two groups

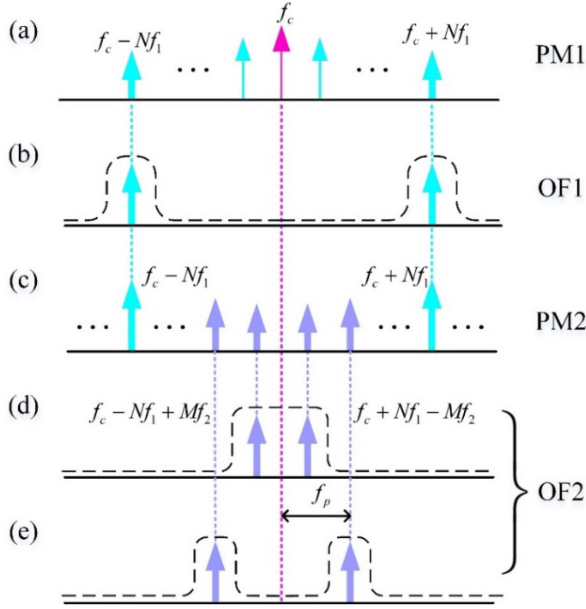


Fig. 2. Spectrum evolution diagram in the double sideband pump light generation part. (a) Spectrum of the signal from PM1. (b) Signal spectrum selected by OF1. (c) Spectrum of the signal from PM2. (d) Signal spectrum selected by OF2 which is a band-pass filter. (e) Signal spectrum selected by OF2 which is a dual-band pass filter.

of optical sidebands around  $f_c \pm Nf_1$  are generated, as shown in Fig. 2(c). OF2 is employed to select a pair of new generated sidebands which are close to the initial optical carrier and have the same order, assuming it is  $M$ . In order to generate the required pump light with specific frequency, OF2 can be a band-pass or a dual-band pass filter, as shown in Fig. 2(d) and (e) respectively. The final double-sideband optical signal can be expressed as:

$$E_{o2}(t) = E_c \left[ J_M(m_2) J_{-N}(m_1) j^{M-N} e^{j(2\pi f_c t - 2\pi N f_1 t + 2\pi M f_2 t - \pi N k t^2)} + J_{-M}(m_2) J_N(m_1) j^{N-M} e^{j(2\pi f_c t + 2\pi N f_1 t - 2\pi M f_2 t + \pi N k t^2)} \right] \quad (1)$$

where  $E_c$ ,  $m_1$  and  $m_2$  are the amplitude of optical carrier, the modulation index of PM1 and the modulation index of PM2, respectively.  $k$  is the chirp rate of  $f_1$  and can be calculated as  $B_1/T$ , in which  $T$  is the period of the signal.

According to the (1), the frequencies and bandwidths of the double-sideband optical signals are  $f_c \pm Nf_1 \mp Mf_2$  and  $NB_1$ , which are determined by the signals generated by MSSs and the orders of sidebands filtered by OFs. The frequency difference between each component of the pump light and the original optical carrier is  $|Nf_1 - Mf_2|$ , and noted as  $f_p$ , which is shown in Fig. 2(e). Meanwhile, the parameter settings in this part should meet certain constraints to avoid spectrum aliasing. When OF2 is a band-pass filter, it should meet the following requirements:

$$f_2 \geq 2f_p + NB_1 + \frac{B_f}{2} \quad (2)$$

where  $B_f$  is the frequency variation range required by OF1 and OF2 to achieve a specific out-of-band suppression ratio.

When OF2 is a dual-band pass filter, it should meet the following requirements:

$$\min(|2Nf_1 - mf_2|) \geq NB_1 + \frac{B_f}{2}, m = 1, 2, 3 \dots \quad (3)$$

The generated double-sideband optical signal can be used as the pump light required for frequency measurement, or can be used to generate broadband interference signal after passing through PD1 to carry out electronic attack, which can be expressed as:

$$I_{PD1}(t) \propto 2[E_c J_N(m_1) J_M(m_2)]^2 \cdot \left\{ 1 + (-1)^{N+M} \cos [2 \cdot |2Nf_1 - 2Mf_2| t + \pi \cdot 2Nkt^2] \right\} \quad (4)$$

From (4), the center frequency of broadband interference signal is  $2|Nf_1 - Mf_2|$ , which is noted as  $f_{PD1}$  and the bandwidth is  $2NB_1$ . Because all the optical modulation in the system is phase modulation, the bias point control is not required and the stability of the system is ensured. And the flexibly tunable pump light signal also ensures the tunability of the waveform generation, so that the proposed method can realize the interference suppression of the corresponding frequency band.

### B. Frequency-to-Power Conversion Part

The frequency-power conversion part is composed of a polarization controller (PC), a phase modulator (PM3), an isolator (ISO), a roll of fiber, an optical circulator and a photodetector (PD2). The spectrum evolution in this part is shown in Fig. 3. Part of the optical signal of the LD is coupled out as the carrier of PM3, where the PC is used to control the polarization state. The unknown RF signal (assuming the frequency is  $f_k$ ) is modulated to the carrier through PM3 to generate the first-order sidebands with the same amplitude and the opposite phase, frequencies of which are  $f_c \pm f_k$ . Then the phase-modulated signal generated by PM3 is used as the probe light to excite SBS. When there are multiple frequency components (assuming the frequency is  $f_{k1}$ ,  $f_{k2}$  and  $f_{k3}$ ) existing in the received unknown signal, the spectrum of the probe light is shown in Fig. 3(a). A pair of pump light at the frequency of  $f_c \pm f_p$  is injected to the port 1 of the optical circulator, and its spectrum is shown in purple line in Fig. 3(b). By conducting the probe light into the optical fiber, the probe light and the pump light are transmitted in opposite direction. ISO is used to prevent the pump light transmitted in the reverse direction. When the frequency difference between the pump light and certain first-order sideband of the probe light is equal to the Brillouin frequency shift  $v_B$  (i.e.,  $f_k = |f_p - v_B|$  or  $f_k = f_p + v_B$ ), the SBS effect will be excited, and the two sidebands of the pump light will produce gain spectrum at the frequency of  $f_c \pm f_p - v_B$ , and loss spectrum at the frequency of  $f_c \mp f_p + v_B$ , as shown in red curve and black curve in Fig. 3(b) respectively. The scattering spectrum on the inner side and the outer side are called internal scattering spectrum (ISS) and external scattering spectrum (ESS) respectively, which all are the effects of SBS. When ISS acts (i.e.,  $f_k = |f_p - v_B|$ ), the

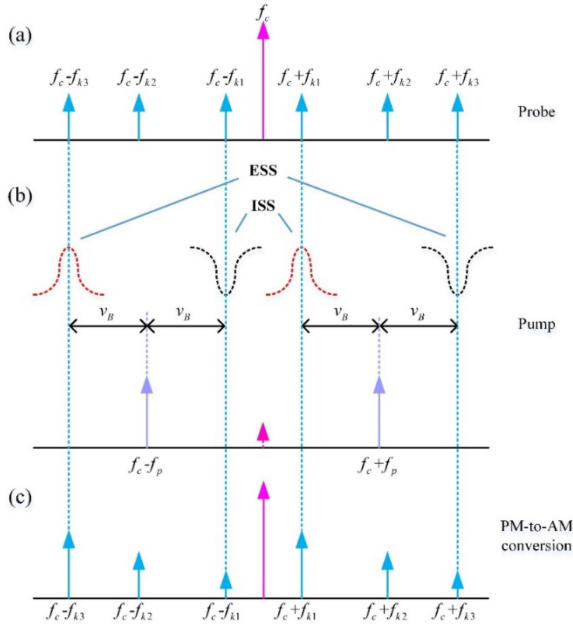


Fig. 3. Spectrum evolution diagram in the frequency-power conversion part. (a) Spectrum of the probe light when it has three unknown signals. (b) The diagram of the internal scattering spectrum (ISS) and external scattering spectrum (ESS) caused by the pump light. (c) The diagram for the PM-to-AM conversion caused by the ISS and ESS.

sidebands at  $f_c - f_{k1}$  and  $f_c + f_{k1}$  are attenuated and gained respectively, so as to realize the conversion of PM-to-AM. The effect of ESS (i.e.,  $f_k = f_p + v_B$ ) is similar, but if the frequency difference between each sideband of the probe light and the pump light is not  $v_B$  (such as  $f_c \pm f_{k2}$ ), the amplitude of the sidebands remains unchanged, as shown in Fig. 3(c). The final optical signal from port 3 of the optical circulator is directly injected to PD2 to generate microwave signal, the frequency of which is  $f_{PD2}$ , and its amplitude can be expressed as:

$$I_{PD2}(t) \propto A_0 (A_1 - A_{-1}) J_0(m_3) J_1(m_3) \cos\left(\omega_k t + \frac{\pi}{2}\right) \quad (5)$$

where  $A_0$ ,  $A_1$  and  $A_{-1}$  are the amplitude of the carrier and the  $\pm 1$ st order sidebands respectively, and  $m_3$  is the modulation index of PM3. According to (5), the amplitude of the microwave signal generated by PD2 is related to the amplitude difference of the first-order sidebands. When the SBS is excited to complete the conversion of PM-to-AM, the amplitude difference will increase, otherwise it will be close to zero. That is, when the SBS is excited, the frequency difference between the pump light and probe light should be  $v_B$ , so as to complete the frequency-to-power conversion. Conversely, the frequency of the unknown signal can be obtained according to the power change.

In the practical frequency measurement application, frequency-sweeping pump light can be employed to measure the unknown signal in certain frequency bands. In this case, it can be judged that SBS is excited according to the moment that the maximum signal amplitude occurs after PD2. When SBS is excited, the pump light and the probe light should meet a certain

frequency relationship ( $f_k = |f_p - v_B|$  or  $f_k = f_p + v_B$ ). The frequency of unknown signal can be calculated according to the frequency of the pump light at this moment and the frequency relationship which should be satisfied to excite SBS. It is worth to mentioned that in order to determine whether ISS or ESS is in action, double sweeping mechanism can be alternated to identify the exact frequency value or a band-pass filter can be used before PM3 for measurement within specific frequency band.

The frequency measurement range of the proposed method mainly depends on the tunable range of the pump light. The proposed method based on optical-domain spectrum manipulation can generate flexibly tunable and ultra-wideband pump light by reasonably setting the parameters of MSS1, MSS2, OF1 and OF2. The frequency measurement covering common radar frequency bands can be realized by using the matching pump light with specific frequencies. In addition, the flexible use of ISS and ESS also expands the frequency measurement range even if the same pump light is used.

Furthermore, the proposed method can complete the frequency measurement and generate the interference signal simultaneously. It can be seen that  $f_{PD1}$  is twice as much as  $f_p$  according to the Section II-A, and the constraint equation between  $f_p$ ,  $f_k$  and  $v_B$  should be  $f_k = |f_p - v_B|$  or  $f_k = f_p + v_B$  according to the Section II-B. Therefore, in most cases, the frequency of the interference signal generated by a sweeping pump light is different from the corresponding frequency measurement range. However, while the frequency of the interference signal is required to cover the frequency measurement range (i.e.,  $f_k = f_{PD1}$ ), two special cases can meet the requirements. The first case is that the frequency measurement range based on ISS is  $\frac{2}{3}v_B \pm \frac{1}{2}B$  and the corresponding interference signal is  $\frac{2}{3}v_B \pm B$  when  $f_p = \frac{1}{3}v_B \pm \frac{1}{2}B$ ,  $B$  is the bandwidth of the sweeping pump light. The second case is that the frequency measurement range based on ESS is  $2v_B \pm \frac{1}{2}B$  and the corresponding interference signal is  $2v_B \pm B$  when  $f_p = v_B \pm \frac{1}{2}B$ .

### III. EXPERIMENTAL RESULTS

According to the diagram in Fig. 1, experimental system is constructed. In the upper path, a light wave with a central wavelength of 1550 nm from the LD (RP-MP-C34-B020-22-0, HAN'S RAYPRO SENSING) is injected into the PM1 (PM-DSES-20-PFA-PFA-UV, EOSPACE) after coupled by the OC1 (50:50). An RF signal generated by the MSS1 (MXG N5183B, KEYSIGHT) is applied to the PM1. The modulated signal is then filtered by the OF1 (WS-16000A-C-S-3-AA-00, FINISAR), amplified to be +10 dBm by the EDFA1 (EDFA-C-LA-20-PM-M, Ovlink), and then injected into the PM2 (MPZ-LN-40, PHOTLINE) which is driven by the RF signal generated by the MSS2 (VSG E8267D, KEYSIGHT). Then the OF2 (XTA-50/U, EXFO) is employed to obtain the pump light, which is amplified to be +13 dBm by the following EDFA2 (EDFA-C-LA-23-PM-M, Ovlink). The pump light is divided into two paths by the OC2 (50:50). One is detected by the PD1 (XPDV2120RA-VF-FA, FINISAR) to generate the broadband interference signal, the other is conducted to the lower path. In the lower path, the polarization state of the light is first adjusted by a PC and then

TABLE I  
MAIN DEVICES EMPLOYED IN THE EXPERIMENTAL SYSTEM AND THEIR PERFORMANCE PARAMETERS

Name	Model	Key parameters
LD	HAN'S RAYPRO SENSING 1550nm Single frequency laser module	Center Frequency: 193.3985 THz Output Power: +13.7 dBm
	RP-MP-C34-B020-22-0	
PM1	EOSPACE PM-DSES-20-PFA-PFA-LV	Half-wave Voltage: 4.1V
PM2	PHOTLINE MPZ-LN-40	Half-wave Voltage: 7V
PM3	EOSPACE PM-DV5-65-PFA-PFA-LV	Half-wave Voltage: 4.1V
MSS1	KEYSIGHT MXG N5183B	Output Power: -12dBm
MSS2	KEYSIGHT VSG E8267D	Output Power: -4dBm
MSS3	KEYSIGHT AWG M8195A	Output Power: 0dBm
OF1	FINISAR WS-16000A-C-S-3-AA-00	Set up according to the needs of the experiment
	EXFO XTA-50/U	Set up according to the needs of the experiment

modulated via the PM3 (PM-DV5-65-PFA-PFA-LV, EOSPACE) which is driven by the unknown RF signal generated by an arbitrary waveform generator (AWG M8195A, KEYSIGHT). After passing through the optical circulator and the ISO respectively, the SBS effect is generated when two counter-propagating lights interact in a roll of fiber (5 km in length). Then the signal is detected by the PD2 (HPDV2120R, FINISAR) and monitored by a real-time spectrum analyzer (RTSA N9040B, Agilent) and a digital storage oscilloscope (DSO, 93204A, Agilent). In order to ensure the signal-to-noise ratio (SNR) of the pump light, microwave amplifiers are employed to amplify the power of the signals from MSS1 and MSS2 to be about +30 dBm to generate high-order sidebands with high power. Table I shows the key parameters of the devices used in the experimental system. The half-wave voltage of PM1 and PM2 should be low enough to obtain high-order sidebands. The SNR of the signals generated by MSS1 and MSS2 should be as high as possible to generate the pump light with high SNR, which can enhance the SBS effect, make the frequency measurement system more sensitive and produce high-quality interference signals. In addition, OF1 and OF2 should have sufficient suppression ratio to suppress unwanted optical sidebands and avoid the interference to frequency measurement. The optical fiber between the circulator and the isolator should have low dispersion or high nonlinearity to excite SBS.

#### A. Frequency Measurement Realization in the Experiment System

According to the principle of the proposed method, it is necessary to measure the amplitude change of the output signal from PD2 to obtain the frequency of unknown RF signal. In

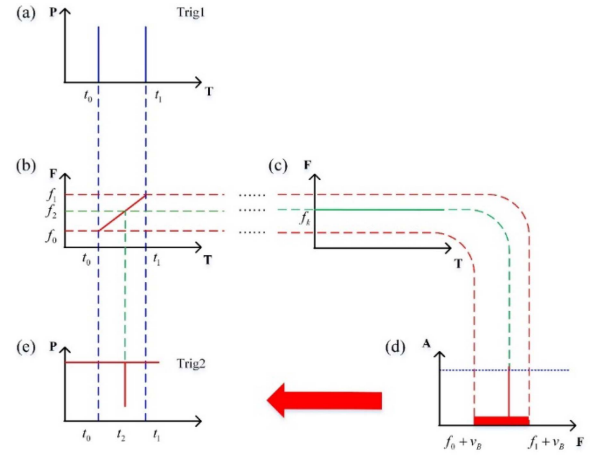


Fig. 4. The realization of frequency measurement by the time-frequency relationship conversion in the proposed system.

the experiment, due to the limitation of the existing devices, DSO is difficult to capture data in a high sampling rate for a long time. Therefore, RTSA and DSO are combined together to complete the frequency measurement. The change of the time-frequency relationship of the experiment system is shown in Fig. 4. Firstly, the MSS1 generates a high-level trigger signal (assuming it is Trig 1) synchronized with the sweeping period, which is delivered directly into the DSO and represents the initial moment of the sweeping period, as shown in Fig. 4(a), in which  $t_0$  and  $t_1$  represent the initial moment of two adjacent sweeping periods, respectively. When the pump light, the period of which is strictly consistent with the Trig 1, sweeps within the frequency of  $f_0 \sim f_1$ , as shown in Fig. 4(b) and assuming the ESS is employed, the corresponding frequency measurement range is  $f_0 + v_B \sim f_1 + v_B$ . At the same time, the RTSA monitors the output of PD2 and outputs the moment when the SBS is excited. If the signal to be measured contains the frequency component  $f_k$ , as shown in Fig. 4(c), SBS will be excited and the output power of PD2 will exceed the preset threshold, as shown in Fig. 4(d). RTSA will generate another trigger signal (assuming it is Trig 2) and send it to the DSO as shown in Fig. 4(e).

Since the initial and terminal moment of Trig 1 correspond to the initial and terminal frequency of the frequency measurement range, the instantaneous frequency of the pump light can be obtained through the relative moment when Trig 2 occurs in the period of Trig 1, and then the frequency to be measured can be calculated according to its relationship with the frequency of the pump light. If there are multiple frequencies existing in this frequency measurement range, the RTSA will generate low-level trigger signals at the corresponding moments respectively, so as to complete the multi-frequency measurement.

#### B. Frequency Measurement With Large Range and High Resolution

The feasibility of the proposed frequency measurement method is firstly verified. In the experiment, the frequency of the unknown signal is set to be 9 GHz and MSS1 generates

TABLE II  
CORRESPONDING FREQUENCY RELATIONSHIP BETWEEN THE MEASUREMENT RANGE, THE PUMP LIGHT AND THE GENERATED INTERFERENCE SIGNAL AND VALUES OF RELATIVE PARAMETERS FOR GENERATING THE PUMP LIGHT

$f_k$ (GHz)	N	M	$f_1$ (GHz)	$f_2$ (GHz)	$f_p$ (GHz)	ESS or ISS	$f_{PD1}$ (GHz)
0.03-5.315	5	3	16.663-17.726	26	5.315-10.6	ISS	10.63-21.2
5.315-10.63	5	3	15.6-16.663	26	0-5.315	ISS	0-10.63
10.63-15.945	5	3	15.6-16.663	26	0-5.315	ESS	0-10.63
15.945-21.26	5	3	16.663-17.726	26	5.315-10.63	ESS	10.63-21.26
21.26-26.575	5	2	16.9685-18.0315	26.47625	31.89-37.205	ISS	63.78-74.41
26.575-31.89	5	2	16.4685-17.5315	22.56875	37.205-42.52	ISS	74.41-85.04
31.89-37.205	6	2	16.0571-16.9429	26.91125	42.52-47.835	ISS	85.04-95.67
37.205-42.52	6	2	17.1571-18.0429	27.55375	47.835-53.15	ISS	95.67-106.3
40-44	6	2	17.7717-18.5217	28	29.37-33.37	ESS	58.74-67.74

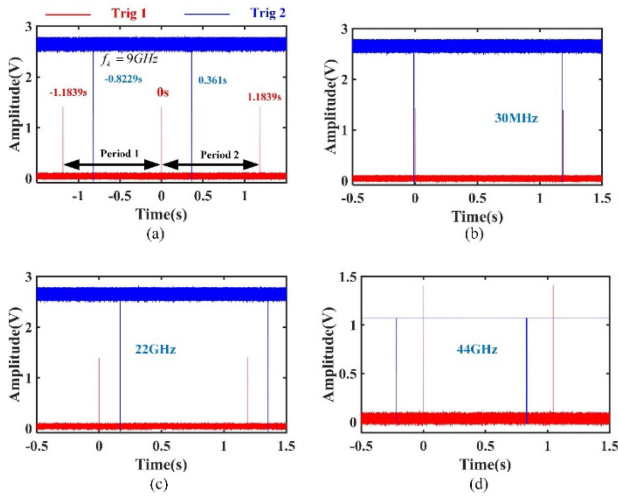


Fig. 5. Frequency measurement diagrams of single frequency signal in wide frequency bands. (a) 9 GHz. (b) 30 MHz. (c) 22 GHz. (d) 44 GHz.

a sweeping microwave signal at the frequency range of 15.6–16.663 GHz, the sweeping period and the frequency sweeping interval of which are 1 s and 5 MHz, respectively. MSS2 generates a single-frequency signal at 26 GHz. The 5th and 3rd order sidebands are selected in the cascade phase modulation by OF1 and F2, respectively. According to  $f_p = |Nf_1 - Mf_2|$ , the sweeping double-sideband pump light at the frequency range of 0–5.315 GHz is generated. In the frequency-to-power conversion part, the  $v_B$  value of 5-km near-zero-dispersion optical fiber is 10.63 GHz. According to  $f_k = |f_p - v_B|$ , the frequency can be measured in the range of 5.315–10.63 GHz. The frequency measurement results of the 9-GHz signal displayed by the DSO is shown in Fig. 5(a). The red line represents Trig 1, which represents the initial moment of each sweeping signal period, and the blue line represents Trig 2, which shows the moment when SBS is excited. According to Fig. 5(a), the frequency of the corresponding pump light is 1.6207 GHz, the frequency to be measured is 9.0093 GHz, and the error is 9.3 MHz.

Furtherly, by tuning the frequency of the signals generated by MSS1 and MSS2 and the sideband orders selected by OF1 and OF2, frequency measurement experiments covering

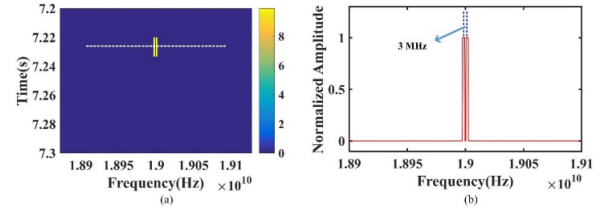


Fig. 6. Frequency measurement resolution calibration of the proposed method. (a) Two trigger signals generated in RTSA corresponding the unknown signals at 18.9985 GHz and 19.0015 GHz. (b) Resolution calibration resulted from the dash line in (a).

common radar bands are carried out. Fig. 5(b)–(d) are the frequency measurement results of single frequency signals at 30 MHz, 22 GHz and 44 GHz respectively, which proves that the proposed system has a large frequency measurement range and can cover the working frequency band of common radars. Table II summarizes the corresponding frequency relationship between the measurement range, the pump light and the generated interference signal and the experimental parameter settings for the desired measurement ranges.

When there are multiple frequency components to be measured which are in the same frequency measurement range, the RTSA will generate low-level triggers at the corresponding moments. Thus, the frequency measurement resolution, an important indicator, is also tested in the experiment, result of which is shown in Fig. 6. The signals to be measured are 18.9985 GHz and 19.0015 GHz, the time-frequency relationship of the trigger signal obtained by the RTSA is shown in Fig. 6(a), and the amplitude along the red dash line in Fig. 6(a) is shown in Fig. 6(b). It is clearly shown that two yellow rectangles which represent that SBS is excited can be distinguished in one frequency sweeping period. It is verified that the proposed system has the ability of multi-frequency measurement, and the frequency measurement resolution can reach 3 MHz. Thus, when the measurement time is not limited and fine enough frequency scanning step ( $< 3$  MHz) is employed, the maximum number of frequency components measured in once measurement course can be calculated by dividing the measurement range by 3 MHz.

Error analysis for frequency measurement is also carried out theoretically and experimentally. Fig. 7 is a schematic diagram

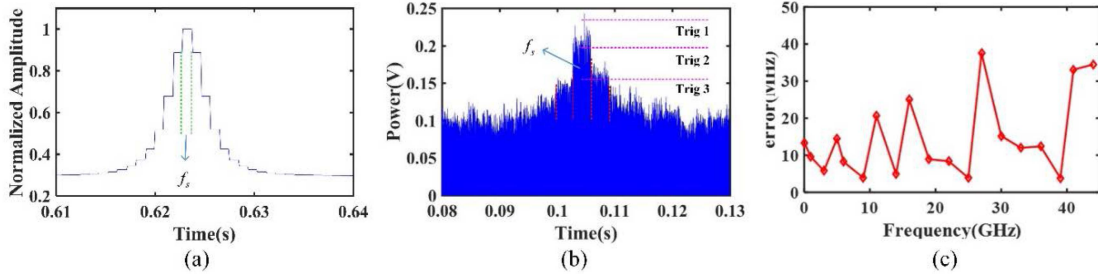


Fig. 7. Measurement error analysis and calibration of the proposed method. (a) Waveform from PD2 in an ideal condition. (b) One actual waveform from PD2. (c) Measurement error value versus the frequency from 30 MHz to 44 GHz.

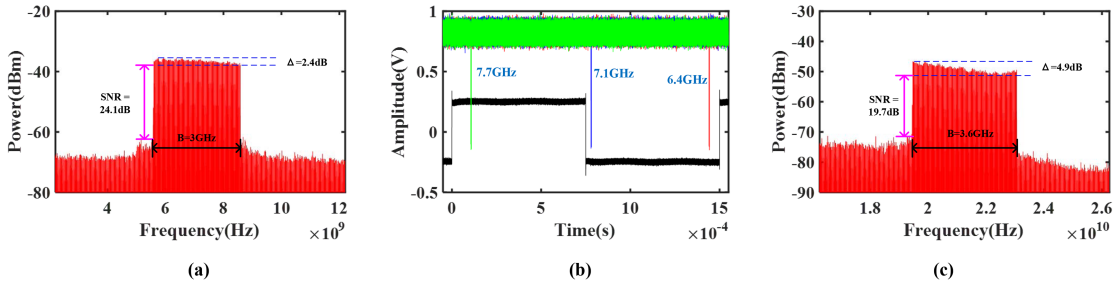


Fig. 8. Simultaneous frequency measurement and interference in two frequency bands. (a) Interference signal generated in 5.5866–8.5866 GHz. (b) Frequency measurement results in the range of 6.3367–7.8367 GHz. (c) Interference signal generated in the range of 23.06–19.46 GHz.

for error analysis. As shown in Fig. 7(a), in an ideal condition, the amplitude reaches the maximum only when the frequency difference between the pump light and the probe light is  $v_B$  in a sweeping period. The moment when the amplitude reaches the maximum corresponds to the only frequency measurement value, and at this very moment the error between the estimated result and the frequency to be measured approaches to be zero. In practice, the sweeping pump light is discontinuous in the frequency domain and its frequency sweeping interval is assumed to be  $f_s$ . The actual waveform from the DSO is shown in Fig. 7(b). Though the variation trend in Fig. 7(b) is generally consistent with the curve in Fig. 7(a), the random variation of the output waveform value in a sweeping interval is still obvious. The moment obtained by RTSA through the trigger threshold may change within the duration of one frequency point, which is also directly influenced by the trigger settings, as shown in Fig. 7(b). When there is a difference of  $v_B$  between the mean value of the two frequencies of the pump light and the frequency of the probe light, the error is the largest. Fig. 7(c) shows the measurement error from 30 MHz to 44 GHz. The sweeping interval setting in the experiment is 5 MHz and the theoretical error should be less than 7.5 MHz ( $1.5f_s$ ). However, the maximum experimental error is 40 MHz, which is mainly due to the random delay introduced by the trigger signal transmission between the RSTA and the DSO and the deviation between the threshold settings.

### C. Simultaneous Frequency Measurement and Interference Signal Generation

As described in Section II-A, by sending the double sideband optical signal from OF2 into PD1, the broadband interference

signal can be obtained, the center frequency and the bandwidth of which are  $2|Nf_1 - Mf_2|$  (i.e.,  $2f_p$ ) and  $2NB_1$  respectively. To demonstrate this ability, the sweeping frequency range of the pump light is set to be 2.7933–4.2933 GHz and the sweeping period is set to be 1.5 ms. Using the ISS of the pump light to measure frequency, the corresponding frequency measurement range is 6.3367–7.8367 GHz. At the same time, the broadband interference signal at the frequency of 5.5866–8.5866 GHz is generated after the PD1, which is shown in Fig. 8(a). Fig. 8(b) shows the measurement result of signals at 7.9 GHz, 7.1 GHz and 6.3 GHz, which identifies the ability for simultaneous frequency measurement and interference signal generation. By setting another set of parameters, the frequency measurement and interference signal generation in the range of 20.36–22.16 GHz can also be achieved at the same time, which is shown in Fig. 8(c). Compared with Fig. 8(a), the signal showed in Fig. 8(c) is at higher frequency and has larger bandwidth. The frequency measurement and interference are completely matched in these two frequency bands, which means the realization of measurement and interference functions in the same microwave photonic system. With the help of photonic integration technology, the system can be carried into applications. For other bands, the frequency relationship between the generated interference signal and the frequency measurement is also summarized in Table II unmatched. Though they are unmatched, other functions can be developed based on the signals from PD1, for example, communication.

## IV. CONCLUSION

This article presents a multifunctional frequency measurement system, which can measure the frequency in a wide range

and with high resolution, and generate broadband interference signals in the corresponding frequency band. The frequency measurement system and waveform generation system share a common pump light generation part, which uses the combination of optical-domain cascade phase modulation and filtering to generate flexible and tunable double-side band pump light, so as to ensure a wide range of frequency measurement and the generation of broadband interference signal. And the advantage of SBS on narrow-band gain is used to enhance the measurement resolution. The feasibility of the system is verified by experiments. The frequency measurement range is 0.03–44 GHz and the error is less than 40 MHz. Multi-frequency measurement is also carried out, and the resolution can reach 3 MHz. In addition, frequency measurement and interference signal generation sharing the same frequency ranges are carried out in 6.3367–7.8367 GHz and 20.36–22.16 GHz. The system can effectively support frequency measurement and electric jamming in a complex electromagnetic environment.

#### REFERENCES

- [1] P. Hannen, *Radar and Electronic Warfare Principles for the Non-Specialist*. IET Digital Library, 2013, pp. 231–242.
- [2] L. Ding, F. Geng, and J. Chen, *Radar Principle*. Beijing, China: PHEI, 2014.
- [3] J. B.-Y. Tsui, *Microwave Receivers With Electronic Warfare Applications*. Hoboken, NJ, USA: Wiley, 1986.
- [4] S. Pan and J. Yao, “Photonics-based broadband microwave measurement,” *J. Lightw. Technol.*, vol. 35, no. 16, pp. 3498–3513, Aug. 2017.
- [5] J. Yao, “Microwave photonics,” *J. Lightw. Technol.*, vol. 27, no. 3, pp. 314–335, Feb. 2009.
- [6] D. Marpaung, J. Yao, and J. Capmany, “Integrated microwave photonics,” *Nature Photon.*, vol. 13, no. 2, pp. 80–90, 2019.
- [7] X. Zou, B. Lu, W. Pan, L. Yan, A. Stöhr, and J. Yao, “Photonics for microwave measurements,” *Laser Photon. Rev.*, vol. 10, no. 5, pp. 711–734, Sep. 2016.
- [8] R. Li, H. Chen, Y. Yu, M. Chen, S. Yang, and S. Xie, “Multiple-frequency measurement based on serial photonic channelization using optical wavelength scanning,” *Opt. Lett.*, vol. 38, no. 22, pp. 4781–4784, Nov. 2013.
- [9] D. Wang et al., “Photonic-assisted microwave frequency measurement with adjustable channel bandwidth based on spectrum-controlled Brillouin phase shift,” *IEEE Photon. J.*, vol. 13, no. 6, Dec. 2021, Art. no. 5500205.
- [10] X. Wang, Y.-L. Yang, Y.-Q. Xu, Y. Cao, and W.-W. Zou, “Power-independent microwave instantaneous frequency measurement based on combination of Brillouin gain and loss spectra,” *IEEE Photon. J.*, vol. 14, no. 4, Aug. 2022, Art. no. 3039507.
- [11] L. V. T. Nguyen and D. B. Hunter, “A photonic technique for microwave frequency measurement,” *IEEE Photon. Technol. Lett.*, vol. 18, no. 10, pp. 1188–1190, May 2006.
- [12] Z. Tu, A. Wen, Y. Gao, W. Chen, Z. Peng, and M. Chen, “A photonic technique for instantaneous microwave frequency measurement utilizing a phase modulator,” *IEEE Photon. Technol. Lett.*, vol. 28, no. 24, pp. 2795–2798, Dec. 2016.
- [13] H. Chi, X. Zou, and J. Yao, “An approach to the measurement of microwave frequency based on optical power monitoring,” *IEEE Photon. Technol. Lett.*, vol. 20, no. 14, pp. 1249–1251, Jul. 2008.
- [14] X. Zou, H. Chi, and J. Yao, “Microwave frequency measurement based on optical power monitoring using a complementary optical filter pair,” *IEEE Trans. Microw. Theory Techn.*, vol. 57, no. 2, pp. 505–511, Feb. 2009.
- [15] H. Emami and M. Ashourian, “Improved dynamic range microwave photonic instantaneous frequency measurement based on four-wave mixing,” *IEEE Trans. Microw. Theory Techn.*, vol. 62, no. 10, pp. 2462–2470, Oct. 2014.
- [16] W. Li, N. H. Zhu, and L. X. Wang, “Brillouin-assisted microwave frequency measurement with adjustable measurement range and resolution,” *Opt. Lett.*, vol. 37, no. 2, pp. 166–168, Jan. 2012.
- [17] S. Zheng, S. Ge, X. Zhang, H. Chi, and X. Jin, “High-resolution multiple microwave frequency measurement based on stimulated Brillouin scattering,” *IEEE Photon. Technol. Lett.*, vol. 24, no. 13, pp. 1115–1117, Jul. 2012.
- [18] Y. Xiao et al., “Multiple microwave frequencies measurement based on stimulated Brillouin scattering with improved measurement range,” *Opt. Exp.*, vol. 21, no. 26, pp. 31740–31750, Dec. 2013.
- [19] H. Jiang et al., “Wide-range, high-precision multiple microwave frequency measurement using a chip-based photonic Brillouin filter,” *Optica*, vol. 3, no. 1, pp. 30–34, Jan. 2016.
- [20] W. Jiao, K. You, and J. Sun, “Multiple microwave frequency measurement with improved resolution based on stimulated Brillouin scattering and nonlinear fitting,” *IEEE Photon. J.*, vol. 11, no. 1, pp. 1–12, Feb. 2019.
- [21] F. Xin, J. Yan, and Q. Liu, “Microwave frequency measurement based on optical phase modulation and stimulated Brillouin scattering,” *Electron. Lett.*, vol. 53, no. 14, pp. 937–939, 2017.
- [22] D. Wang et al., “Instantaneous microwave frequency measurement with high-resolution based on stimulated Brillouin scattering,” *Opt. Laser Technol.*, vol. 113, pp. 171–176, 2019.
- [23] D. Wang et al., “Wide-range, high-accuracy multiple microwave frequency measurement by frequency-to-phase-slope mapping,” *Opt. Laser Technol.*, vol. 123, 2020, Art. no. 105895.
- [24] L. V. T. Nguyen, “Microwave photonic technique for frequency measurement of simultaneous signals,” *IEEE Photon. Technol. Lett.*, vol. 21, no. 10, pp. 642–644, May 2009.
- [25] T. A. Nguyen, E. H. W. Chan, and R. A. Minasian, “Instantaneous high-resolution multiple-frequency measurement system based on frequency-to-time mapping technique,” *Opt. Lett.*, vol. 39, no. 8, pp. 2419–2422, Apr. 2014.
- [26] S. Wang, Y. Sun, J. Chen, and G. Wu, “Broadband photonic RF channelization based on optical sampling pulse shaping,” *IEEE Photon. Technol. Lett.*, vol. 32, no. 18, pp. 1195–1198, Sep. 2020.
- [27] D. Wang, X. Zhang, X. Zhao, Z. Yang, and W. Dong, “Photonic microwave frequency measurement with improved resolution based on bandwidth-reduced stimulated Brillouin scattering,” *Opt. Fiber Technol.*, vol. 68, 2022, Art. no. 102803.
- [28] T. Shi and Y. Chen, “Multiple radio frequency measurements with an improved frequency resolution based on stimulated Brillouin scattering with a reduced gain bandwidth,” *Opt. Lett.*, vol. 46, no. 14, pp. 3460–3463, Jul. 2021.